A REVIEW OF OCEANIC SALT-FINGERING THEORY

by

Eric Kunze
APL, U of Washington
1013 NE 40th
Seattle, WA 98105-6698

accepted by *Prog. Oceanogr.*, JUN 2001

Abstract

Salt-fingering is a potentially important mechanism for mixing different water-masses in those parts of the ocean where warm salty waters overlie cooler fresher. This review surveys advances in salt-fingering theory as they pertain to ocean mixing. Basic equations are presented along with steady, maximum buoyancy-flux and fastest-growing finger solutions. Attempts to theoretically quantify finger-induced fluxes of heat, salt and buoyancy, and to understand staircase formation and maintenance, are described. Also considered are the confounding influences of internal wave shear and strain, and intermittent internal-wave shear-driven turbulence, which are present in the ocean but in few theories. Finally, outstanding theoretical questions about the role of salt fingers in the ocean are raised.

Keywords: salt fingers, double diffusion, mixing, microstructure, water-masses

1. Introduction

The density of ocean waters depends on variations in both potential temperature θ and salinity *S* which molecularly diffuse at different rates. Where density is stably stratified in the vertical (light water overlying heavy) but unstably stratified in one of its components, double-diffusive instability can give rise to mixing of different water-masses. In heat-salt double diffusion, the potential energy locked in the unstable component is released through the more rapid molecular diffusion of heat than salt (Stern 1960). This process occurs on molecular scales O(1 cm) but impacts much larger scales by efficiently mixing water-mass properties.

If salt is the destabilizing component (warmer saltier water overlying cooler fresher), the instability takes the form of tightly packed blobs of sinking salty and rising fresh water referred to as salt fingers. Salt fingers efficiently flux salt vertically and could be likened to liquid alveoli in that diffusion is amplified by the convolving isotherms and isohalines on microscales (Winters and D'Asaro 1996). Much of the upper ocean Central Waters at tropical, subtropical and mid-latitudes are fingering favorable. At a few sites, such as east of Barbados (Mazeika 1974; Boyd and Perkins 1987), below the Mediterranean salt tongue (Howe and Tait 1970; Elliott *et al.* 1974) and in the Tyrrhenian Sea (Johannessen and Lee 1974; Zodiatis and Gasparini 1996), where destabilizing salinity gradients almost compensate stabilizing temperature gradients, the stratification takes the form of thermohaline staircases with O(10 m) thick well-mixed layers alternating with O(1 m) thick high-gradient interfaces.

This paper reviews salt-fingering theory with an emphasis on aspects relevant to characterizing salt-finger microstructure and fluxes in the ocean. Observational evidence for salt fingers in the ocean is summarized in Schmitt (2000 this issue) and a review of salt-finger numerical simulations given by Yoshida and Nagashima (2000 this issue). Theoretical and observational aspects of double-diffusive intrusions, which are often driven by salt-finger fluxes, are described by Ruddick and Kerr (2000 this issue) and Ruddick and Richards (2000 this issue), respectively.

Section 2 introduces the fundamental equations of motions for tall thin salt fingers. General solutions are presented in section 3, while steady, maximum buoyancy-flux and fastest-growing salt-fingers are discussed in sections 4 and 5, respectively. Section 6 reviews efforts to quantify salt-finger fluxes theoretically for both the laboratory and ocean. Section 7 briefly considers the formation and maintenance of thermohaline staircases which are observed in regions of the ocean where the density ratio $R_\rho = \alpha \overline{T_z} / \beta \overline{S_z}$ is less than 1.7. Interactions of salt-finger with finescale internal-wave shear and strain, and intermittent internal-wave-shear-driven turbulence, are discussed in Section 8. Finally, I present outstanding theoretical questions that must be addressed before we can fully understand salt fingers in the ocean.

2. Equations of Motions

The equations of motion for tall, narrow ($\partial/\partial z << \partial/\partial x, \partial/\partial y$) salt fingers growing in uniform background vertical gradients were first derived by Stern (1960)

$$w_t = g(\alpha T' - \beta S') + \nu\nabla^2 w$$

$$T'_t + w\overline{T_z} = \kappa_T \nabla^2 T' \quad (1)$$

$$S'_t + w\overline{S_z} = \kappa_S \nabla^2 S'$$

where w, T' and S' are the fingers' vertical velocity, temperature and salinity perturbations relative to a horizontal average, $\overline{T_z}$ and $\overline{S_z}$ are average vertical temperature and salinity gradients (possibly modified by the fingers), $\nabla^2 = \partial^2/\partial x^2 + \partial^2/\partial y^2$ the horizontal Laplacian, ν the molecular viscosity, κ_T the molecular diffusivity of heat, and κ_S the molecular diffusivity of salt. For growing salt-finger instabilities, both background temperature $\overline{T}(z)$ and salinity $\overline{S}(z)$ must decrease with depth (Stern 1960) and the density ratio $R_\rho = \alpha\overline{T_z}/\beta\overline{S_z}$ must be less than the diffusivity ratio $\kappa_T/\kappa_S = 100$ (Huppert and Manins 1973). The quantity $g(\alpha T' - \beta S')$ is the buoyancy anomaly b' which induces vertical motions of the fingers. The buoyancy anomaly is created by more rapid diffusion of heat than salt between adjacent fingers, warming cool fresh anomalies to make them lighter, and cooling warm salty anomalies to make them heavier, than the adjacent fluid. For high Prandtl number $\nu/\kappa_T >> 1$ ($\simeq$ 7 in the ocean), the viscous term in the vertical momentum equation greatly exceeds the vertical acceleration w_t which can be neglected for all but density ratios $R_\rho - 1$ much less than $\kappa_T^2/(4\nu^2) = 0.0025$ which are not realized in the ocean. Schmitt (1979b) overcame the increased complexity as density ratio R_ρ approaches 1 by posing the problem in terms of flux ratio $R_F =$

$\langle w\alpha T' \rangle / \langle w\beta S' \rangle$. For the oceanic range of density ratios ($R_\rho \geq 1.4$), the vertical momentum equation reduces to a balance between the buoyancy anomaly and viscous drag. For high diffusivity ratios, $\kappa_T/\kappa_S >> 1$ (κ_T/κ_S = 100 in ocean), the diffusive term in the salinity equation can be neglected for density ratios R_ρ much less than κ_T/κ_S for many problems.

3. General Solutions

Assuming either that (i) salt diffusion extends across the entire finger width or (ii) fingers are of finite height growing in uniform background gradients, solutions for the above equations can be found for horizontal planforms that are square $e^{\sigma t}\sin(k_x x)\sin(k_y y)$, sheet $e^{\sigma t}\sin(k_x x)$, or a combination of the two that can take the form of triangles, hexagons or asymmetric plumes (Schmitt 1994). Here, σ is the growth rate, and k_x and k_y are horizontal wavenumbers. While Proctor and Holyer (1986) found that sheets were the most stable mode, a more careful analysis by Radko and Stern (2000) has demonstrated that square planform fingers are the most stable, consistent with laboratory findings. Well-ordered fingers are observed in laboratory and numerical experiments at high density ratios but become increasingly disordered at low R_ρ. Growth rates σ are positive for density ratios R_ρ less than the diffusivity ratio (inverse Lewis number) κ_T/κ_S and for horizontal wavenumbers

$$k = \frac{2\pi}{\lambda} < \sqrt[4]{\frac{(\kappa_T - R_\rho \kappa_S) g \beta \bar{S}_z}{4\nu\kappa_T\kappa_S}} \qquad (2)$$

(Fig. 1). For any given density ratio R_ρ, maximum growth rates occur at intermediate wavelengths (dashed curve) due to competition between destabilizing heat diffusion and stabilizing viscous drag, both of which intensify at smaller scales. Maximum growth rates increase as density ratios R_ρ approach 1.

Figure 2 displays the ratio $R_F = \langle w'\alpha T'\rangle / \langle w'\beta S'\rangle$ of heat-flux to salt-flux contributions to the buoyancy-flux as a function of density ratio R_ρ and horizontal wavelength λ. Heat-salt laboratory experiments (corrected for molecular diffusion of heat through the interface and tank sidewalls) typically find flux ratios of 0.6-0.65 (Fig. 3; Turner 1967; Schmitt 1979a; Taylor and Bucens 1989), consistent with fastest-growing finger flux ratios; McDougall and Taylor (1984) and Linden (1973) reported lower values, suggesting a possible contribution from steady fingers or fingers of maximum buoyancy-flux under some circumstances (see later). Schmitt *et al.* (1987) inferred flux ratios of 0.85 in the thermohaline staircase east of Barbados based on the lateral density ratio of the homogeneous layers. The oceanic values were argued to be a combination of fastest-growing finger flux ratio and either (i) turbulence with flux ratio $R_F = R_\rho = 1.6$ (Marmorino 1990; Fleury and Lueck 1991), or (ii) nonlinearity in the seawater equation of state influencing the flux divergence and so elevating the flux ratio (McDougall 1991).

Theoretical studies have focussed on fastest-growing, steady and spectral descriptions of salt fingers. Investigations of fastest-growing fingers (Stern 1975; Schmitt 1979b; Kunze 1987) have been motivated by the close match of the fastest-growing flux ratio with laboratory and numerical simulation flux ratios (Fig. 3), as well as the expected long-time dominance of fastest-growing fingers. The spectral approach recognizes that a range of scales is likely to be present, and that fingers may break down due to secondary instability before fastest-growing fingers dominate, particularly at low density ratio (Gargett and Schmitt 1982; Shen and Schmitt 1995). Allowing finger heights at all wavelengths not to exceed a fixed length, Shen and Schmitt (1995) derived a finger wavenumber spectrum for temperature gradient with a + 2 slope, consistent with observations (Marmorino 1987; Mack 1989) albeit with either fluxes or interface thicknesses inconsistent with oceanic values. Theoretical work to date has neglected finger/finger interactions.

4. Steady Solutions

Steady models have been developed for thin interfaces sandwiched between homogeneous layers on the grounds that, because of the interface's finite thickness, these are expected to evolve quickly to steady state (Stern 1976; Joyce 1982; Howard and Veronis 1987; 1992; Shen 1993). Stern (1976) examined the steady solution, choosing the wavenumber $[g\alpha \overline{T}_z/(4\nu\kappa_T)]^{1/4}$ that produced maximum buoyancy-flux for a given ΔS; this is not the same as the steady finger wavenumber in the previous section. The associated flux ratio was 0.2-0.25. Because salt diffusion is negligible, fingers connecting homogeneous reservoirs do not have sinusoidal salt structure. Howard and Veronis (1987) examined this structure for steady fingers of maximum buoyancy-flux extending between two homogeneous reservoirs in the limit of very small salt diffusivity $\kappa_S/\kappa_T << 1$, obtaining similarity solutions for the boundary layers between adjacent fingers. They again found flux ratios of ~ 0.25. This flux ratio is considerably less than the values greater than 0.5 found in most lab experiments. However, Shen (1993) points out that steady models can yield a flux ratio ~ 0.5 when the wavenumber that maximizes finger velocity rather than buoyancy-flux is used. Maximizing velocity is equivalent to maximizing the growth rate in the limit that salt diffusion extends across the fingers.

Howard and Veronis (1992) examined the stability of steady fingers of maximum buoyancy-flux as a function of a nondimensionalized salinity step, or finger aspect ratio, $Q = \beta\Delta S/(\lambda_b \alpha \overline{T}_z) = R_\rho^{-1}(\ell_i/\lambda_b)$ where $\lambda_b = [4\nu\kappa_T/(g\alpha\overline{T}_z)]^{1/4}$ is the buoyancy-layer scale and ℓ_i the interface thickness. They found that the dominant instability switched from being oscillatory involving viscosity and heat diffusivity for $Q < \nu/\kappa_T$ (short fingers) to pure real due to shear between adjacent fingers ∇w at higher Q (tall fingers).

Relaxing the condition that the fingers be tall and narrow (e.g., Howard and Veronis 1987), additional terms must be included in the equations of motion such as the vertical pressure gradient p_z in the vertical momentum equation, vertical diffusion $\kappa\partial^2/\partial z^2$, and horizontal advection of temperature and salinity, particularly at finger tips. These additional terms could play an important role at low density ratios, where fingers are short and stubby rather than tall and narrow, or for fingers evolving in thin high-gradient interfaces sandwiched between two homogeneous layers as characterizes most lab and numerical experiments. Numerical simulations under these conditions show formation of bulbous tips resembling mushrooms where the fingers intrude into the adjacent homogeneous layers (Fig. 4; Shen 1989; Shen and Veronis 1997). The resulting structure and flux ratios depend on the destabilizing salinity step across the interface ΔS as well as the density ratio R_ρ.

Presumably, there is also dependence on the thickness of the high-gradient interface ℓ_I through Q (see earlier).

5. Fastest-Growing Fingers

In the remainder of this review of salt-fingering theory, the focus will be on fastest-growing fingers of sinusoidal horizontal structure because flux ratios and wavelengths observed in most laboratory experiments (Turner 1967; Linden 1973; Schmitt 1979a; McDougall and Taylor 1984; Taylor and Bucens 1989) and numerical simulations (Shen 1993; 1995) are consistent with dominance of fastest-growing fingers (Fig. 3). Microstructure tows in the ocean also find horizontal wavenumbers consistent with fastest-growing fingers (Magnell 1976; Gargett and Schmitt 1982; Lueck 1987; Marmorino 1987; Mack and Schoeberlein 1993). Uniform background vertical gradients will be assumed since thin interfaces appear to be atypical of the ocean (Linden 1978; Kunze 1987). Advection can then create sinusoidal salt structure in the horizontal -- unlike the case of a thin interface between two homogeneous reservoirs where the horizontal structure for salt can only be sinusoidal if diffusion spans the width of a finger (Shen 1993). Numerical simulations find tall well-ordered fingers at high density ratio, becoming shorter and more disordered as the density ratio approaches one, more closely resembling a field of rising and sinking blobs that collide and maneuver around each other. Shen (1993) suggested that collisions between rising and sinking blobs set the terminal velocity of the fingers. But by tracking individual blobs, Merryfield and Grinder (2001) found that linear viscous drag and nonlinearity were the controlling factors.

Theory readily identifies the fastest-growing salt-fingering wavenumber

$$k_{fg} = \frac{2\pi}{\lambda} = \sqrt[4]{\frac{g\beta\bar{S}_z(R_\rho - 1)}{\nu\kappa_T}} \tag{3}$$

(Fig. 5), associated growth rate

$$\sigma_{\max} = \frac{1}{2}\sqrt{\frac{(\kappa_T - R_\rho\kappa_S)g\beta\bar{S}_z}{\nu}}\left(\sqrt{R_\rho} - \sqrt{R_\rho - 1}\right), \tag{4}$$

(Fig. 6) and flux ratio

$$R_F = \frac{\alpha F_T}{\beta F_S} = \frac{\alpha\langle w'T'\rangle}{\beta\langle w'S'\rangle} = \sqrt{R_\rho}\left(\sqrt{R_\rho} - \sqrt{R_\rho - 1}\right) \tag{5}$$

(Fig. 3) as functions of salinity gradient $\bar{S}_z = \partial\bar{S}/\partial z$ and density ratio $R_\rho = \alpha\bar{T}_z/\beta\bar{S}_z$ (Stern 1960; 1975; Schmitt 1979b; Kunze 1987). Walsh and Ruddick (2000) find that a decreasing flux ratio with density ratio produces an instability of increasing growth rate with decreasing vertical scale.

6. Fluxes

Of principal interest to the oceanographic community at large are the heat- and salt-fluxes produced by salt fingers since these modify water-masses. Quantifying these fluxes is difficult, requiring knowledge of what limits the growth of fingers to finite amplitude. This was originally attempted through laboratory experiments in which heat- and salt-fluxes were measured between two well-mixed layers separated by a thin fingering-favorable interface (Turner 1967; Linden 1973; Schmitt 1979a; McDougall and Taylor 1984; Taylor and Bucens 1989). The heat- and salt-fluxes were found to depend only on the salinity step across the interface ΔS and the density ratio R_ρ

$$
\begin{aligned}
g\beta F_S &= c\,[g\beta\Delta S]^{4/3} f(R_\rho) \\
g\alpha F_T &= R_F \cdot g\beta F_S
\end{aligned}
\qquad (6)
$$

where the constant $c = 0.085$ was evaluated from solid-plane flux experiments (Turner 1967). Laboratory flux ratios R_F are in agreement with the theoretical expression for fastest-growing fingers (3) in the Turner (1967), Schmitt (1979a) and Taylor and Bucens (1989) work but lower in Linden (1973) and McDougall and Taylor (1984) experiments. The $\Delta S^{4/3}$ flux law (6) arises from dimensional reasoning under the proviso that the interface thickness is unimportant (Turner 1967; Radko and Stern 2000). Application of this $\Delta S^{4/3}$ flux law is hampered in most of the fingering-favorable ocean by the absence of well-defined layers and interfaces so that the salinity step ΔS cannot be plausibly quantifiable. Even in well-defined staircases, the lab $\Delta S^{4/3}$ flux laws have been found to overestimate fluxes by over an order of magnitude (Gregg and Sanford 1987; Lueck 1987; Kunze 1987; Hebert 1988; Bianchi *et al.* 2002), because the high-gradient interfaces are thicker than lab predictions (Linden 1978; Kunze 1987); in contrast, the high-gradient interfaces in the ocean's diffusively convective staircases are as thin as expected (Padman and Dillon 1987) so the absence of thin interfaces is not due inadequate sensor resolution.

In continuous background stratification, Stern (1969) argued on dimensional grounds that the maximum ratio of the buoyancy-flux $<w'b'>$ to νN^2 should be

$$\frac{<w'b'>}{\nu N^2} \sim O(1) \tag{7}$$

where ν is the molecular viscosity and N the buoyancy frequency. This nondimensional limit on the magnitude of salt-finger fluxes has come to be known as the Stern number or *collective instability* criterion. Stern suggested that finger energy would be lost to larger-scale oscillations of wavenumber K. More rigorously, Holyer (1981) demonstrated secondary instability of steady ($\sigma = 0$) fingers to oscillatory long internal-wave oscillations of very low aspect ratio K_x/K_z if the Stern number $<w'b'>/\nu N$ exceeds 1/3. Holyer (1984) confirmed that collective instability is the fastest-growing provided the Prandtl number ν/κ_T is very large, $(\nu/\kappa_T)\ (\kappa_S/\kappa_T)\ (K_x^2/K^2)[(R_\rho - 1)/(1 - R_\rho \kappa_S/\kappa_T)] >> 1$, and $K^2 << k^2$. However, for the heat-salt system, she identified a different nonoscillatory instability with $(K_x, K_z) = (0, 0.3)k_x$ which grew ten times faster than collective instability. Shen (1995) showed that 2-D fingers are shear-unstable at all wavenumbers, not just the steady fingers examined by the above investigators. Fingers in uniform background gradients tend to be disorganized, achieving a steady state with a stationary Stern number (7) only in a statistical sense (Shen 1993; 1995). Rather than being a universal constant, the critical Stern number appears to be a function of density ratio R_ρ, Prandtl number ν/κ_T and Lewis number κ_S/κ_T. While heat-salt lab experiments find Stern numbers O(1), sugar-salt experiments find values of 0.002-0.006 (Lambert and Demenkow 1971; Griffiths and Ruddick 1980).

Kunze (1987) suggested that finger amplitudes could be limited by secondary instability for unity finger Froude number

$$Fr_f = \frac{|\nabla w|}{N} \sim \mathrm{O}(1) \qquad (8)$$

in which the usual vertically-sheared horizontal velocity $|\mathbf{V}_z|$ is replaced by horizontally-sheared vertical velocity $|\nabla w|$. As in Miles and Howard (1961), this corresponds to when the shear contains sufficient kinetic energy to overcome the potential energy of the stratification. It does not take into account possible damping of any instability by molecular processes (see section 2).

For fastest-growing fingers, the finger Froude number (8) is virtually identical to the Stern number except very near density ratios of $R_\rho = 1$; a Reynolds number criterion $w\lambda/\nu \sim \mathrm{O}(1)$ yields a similar constraint (Stern 1969). Applied to gradients in oceanic fingering-favorable regions, the Stern, or finger Froude, number constraint predicts fluxes

$$g\alpha F_T = g\alpha\langle w'T'\rangle = \frac{Fr_C{}^2\sqrt{C_T}}{\sqrt{C_w}\,2\sigma t_{\max}}\ \nu g\beta\bar{S}_z\left[\sqrt{R_\rho}\left(\sqrt{R_\rho} + \sqrt{R_\rho - 1}\right)\right]$$

$$g\beta F_S = g\beta\langle w'S'\rangle = \frac{Fr_C{}^2\sqrt{C_S}}{\sqrt{C_w}\,2\sigma t_{\max}}\ \nu g\beta\bar{S}_z\left[\left(\sqrt{R_\rho} + \sqrt{R_\rho - 1}\right)^2\right], \qquad (9)$$

where Fr_C is the critical finger Froude number, C_w, C_T and C_S are O(1) geometric constants associated with the horizontal planform structure (= 0.25 for square planform fingers, 0.5 for sheets), and the time-average factor

$$2\sigma t_{\max} = \ln\left[\frac{8\nu Fr_c{}^2}{C_w \kappa_T} \sqrt{R_\rho - 1}\left(\sqrt{R_\rho} + \sqrt{R_\rho - 1}\right)^3\right] \qquad (10)$$

for exponential growth from perturbations of aspect ratio one initially. The above flux laws counterintuitively predict larger fluxes for higher density ratios despite faster growth rates at low density ratios. As discussed later, slower growing fingers at high density ratios may be disrupted and suppressed by intermittent turbulence and other processes in the ocean so that faster-growing fingers at low density ratios dominate. Walsh and Ruddick (1995) find that the above flux law creates an instability that grows without bound as its vertical scale approaches zero (ultraviolet catastrophe).

This criterion (9-10) predicts fluxes of comparable magnitude to those inferred from many oceanic microstructure observations (Gargett and Schmitt 1982) and largescale budgets (Hebert 1988; Bianchi *et al.* 2002). In particular, it produces fluxes comparable to those found in the thermohaline staircase east of Barbados (Gregg and Sanford 1987; Lueck 1987; Marmorino *et al.* 1987). However, its predictions are a factor of 30 smaller than fluxes deduced by St. Laurent and Schmitt (1999) in the eastern N. Atlantic. St. Laurent and Schmitt carefully binned shear and temperature microstructure with respect to density ratio and Richardson number. They used gradients smoothed over 5 m which could bias model fluxes low if unresolved permanent layering finestructure is present. Their average fluxes were dominated by contributions from low density ratio and high Richardson number (see section 8.2).

Equating the high-gradient interface thickness ℓ_i to the maximum finger height $h_{\max}$, the Stern or finger Froude number constraint reproduces laboratory heat-salt $\Delta S^{4/3}$ flux laws except at density ratios $R_\rho < 2$ where fluxes are underpredicted by factors of 2-3 (Figs. 7 and 8; Kunze 1987; Shen 1993). This criterion implies interface thicknesses $\ell_i \sim 0.3$ m, an order of magnitude smaller than the 2-5 m thickness typically observed in oceanic staircases (Linden 1978; Boyd and Perkins 1987).

Numerical simulations are gradually becoming capable of simulating salt fingers for oceanic Prandtl and Lewis numbers though even two-dimensional simulations of heat-salt fingers have been limited to domains a few fingers wide (Shen 1995; Merryfield and Grinder 2001) and 3-D simulations cannot yet handle the heat-salt system (Stern *et al*. 2001). While Shen (1995) did not compare his modelled fluxes with observations, we will attempt to do so here. Their fluxes (Fig. 9) are considerably higher than those from (9)-(10) (Figs. 7 and 8) for density ratios $R_\rho < 3$, thus comparable with those inferred by St. Laurent and Schmitt (1999) and over an order of magnitude higher than those inferred in the staircase east of Barbados

(Gregg and Sanford 1987; Lueck 1987; Marmorino *et al.* 1987). For unbounded background gradients, Radko and Stern (1999) and Stern *et al*. (2001) found that 3-D numerical simulations yield finger fluxes 2-3 times higher (Nusselt numbers $Nu = F_T / \kappa_T \overline{T_z}$ of 43 and salt diffusivities of 0.2×10^{-4} m^2 s^{-1} for the conditions found in the eastern N. Atlantic) than 2-D simulations (Fig. 9). The 3-D instability is not collective instability but arises from lateral salinity gradients and transfers energy to vertical scales similar to finger horizontal scales. Their fluxes were proportional to background vertical gradients $\overline{S_z}$ and $\overline{T_z}$. In contrast, Radko and Stern's (2000) simulations bounded above and below by rigid boundaries produced fluxes proportional to $\Delta S^{4/3}$ and independent of domain dimension and height.

7. Staircase Lengthscales

With linear dependence on the salinity gradient $\overline{S_z}$ across the interface in (9), oceanic fingering fluxes in staircases should depend both on (i) the layer thickness L_o, which establishes the interfacial salinity step $\Delta S = <\overline{S_z}> (L_o + \ell_i)$ in a largescale smoothed salinity gradient $<\overline{S_z}>$, and (ii) the interface thickness ℓ_i which determines the interfacial gradient $\overline{S_z} = \Delta S/\ell_i = <\overline{S_z}>(L_o + \ell_i)/\ell_i$ [$\simeq <\overline{S_z}>L_o/\ell_i$ for a staircase with $L_o >> \ell_i$].

What controls layer and interface staircase thicknesses in the ocean is not known. While staircase formation has traditionally been thought of as a 1-D instability induced by collective instability (Stern 1969), metastable equilibria (Stern and Turner 1969) or the countergradient double-diffusive buoyancy-fluxes (Stern and Turner 1969; Schmitt 1994; Özgökmen *et al.* 1998), it may also arise from horizontal interleaving (Merryfield 2000; Ruddick and Kerr 2000 this issue); sites of prominent staircases are also regions of largescale horizontal water-mass gradients. Horizontal intrusions may also explain the alternating diffusive and fingering layers that extend across entire basins in the Arctic Ocean, crossing different water-masses and water-ages with impunity (Carmack *et al.* 1997). Merryfield (2000) explored the 1- and 2-D hypotheses, coming to the conclusion that 1-D mechanisms required solid boundaries above and below, or large imposed disturbances to the stratification, to induce sufficiently strong buoyancy-flux divergences to form a staircase. In the case of the countergradient buoyancy-fluxes, Merryfield found no preferred scale for staircase steps; they grew indefinitely. On the other hand, his simulations of 2-D double-diffusive intrusions formed thermohaline staircase structure for low density ratio and turbulent mixing rates as observed.

Given the persistence and invariance of oceanic thermohaline staircase structures over at least 25 years (Schmitt 1995; Zodiatis and Gaspirini 1996), staircases have more than enough time to establish thin $\Delta S^{4/3}$ flux law interfaces. A range of interface thicknesses were found in the thermohaline staircase east of Barbados, including a few of O(0.1 m). However, the bulk of the interfaces were 2-5 m thick, an order of magnitude too large for $\Delta S^{4/3}$ flux laws to apply (Linden 1978; Kunze 1987).

Kelley's (1984) scaling for layer thickness $H = \sqrt{\kappa_T/N} \cdot f(R_\rho, \nu/\kappa_T, \kappa_T/\kappa_S)$ and eddy diffusivity $K_T = cfRa^{1/3}\kappa_T$ appears to work well for diffusively-unstable staircases. One might blindly replace the molecular diffusivity of heat κ_T with the fingering salt diffusivity $F_S/\langle S_z\rangle$. However, using observed microstructure estimates of the salt-flux (Gregg and Sanford 1987; Lueck 1987) underestimates the layer thicknesses. Interestingly, a laboratory-inferred $\Delta S^{4/3}$ salt-flux (6) produces layer thicknesses of the right order of magnitude. Merryfield's (2000) double-diffusive intrusion model also reproduces observed step thicknesses (layer plus interface) but he did not discuss layer and interface thicknesses separately.

8. Different Fluxes in the Lab and Ocean

Why are oceanic fluxes so much weaker, or equivalently, oceanic interfaces so much thicker, than those found in laboratory experiments and numerical simulations? Most laboratory and numerical experiments have been initialized as two homogeneous layers separated by a very thin interface which is allowed to thicken under the influence of fingers. In the ocean, the initial state is probably better-described as one of continuous stratification. Numerical simulations by Stern and Radko (1999) and Merryfield (2000) suggest that, by themselves, salt fingers can only create steps if flux divergences are externally forced by rigid boundary conditions or large perturbations to the stratification. But, once created, these evolve toward thinner interfaces with $\Delta S^{4/3}$ fluxes across them (Stern and Turner 1969; Linden 1978; Özgökmen *et al*. 1998; Radko and Stern 2000). This suggests that some additional process present in ocean staircases but not in idealized experiments prevents interfaces from thinning. Possible candidates include finescale internal wave shear and strain fluctuations, and intermittent internal wave-driven turbulence.

8.1. interaction with internal-wave strain ξ_z

Internal-wave vertical divergence $\partial w/\partial z = \partial(\xi_z)/\partial t$ would act to stretch and squash the fingering environment and possibly rectifying fluxes, depending on the relative timescales of the strain ξ_z and finger adjustment. Lab experiments by Stamp *et al*. (1998) found that feedback between internal wave strain and diffusive instability organized the convective motions and fed energy into internal waves. This process has yet to be explored in an oceanic parameter regime or for salt fingers. Straining may also intermittently create thin interfaces for sufficient durations for large fluxes to develop.

8.2. interaction with internal-wave vertical shear $\boldsymbol{V}_z$

Vertical shear $\boldsymbol{V}_z = (U_z, V_z)$ will act to tilt square planform salt fingers. Linden (1974) demonstrated in the lab and analytically (see also Thangam *et al*. 1984) that, in steady rectilinear shear U_z, fingers formed vertical sheets $\sin(k_y y)$ aligned with the shear. Linden reported the fluxes to be unaltered by the presence of vertical shear.

Finescale vertical shear in the ocean is dominated not by steady but by O(N) amplitude near-inertial internal wave fluctuations. These rotate clockwise in time with a timescale of f^{-1}, where $f = 2\Omega\sin(\mathrm{lat}°)$ is the Coriolis frequency, and turn either clockwise and anticlockwise with depth, e.g., $(u_z\ ,\ v_z\ ) = V_z\ [\cos(k_z z - \omega t)\ ,\ \sin(k_z z - \omega t)\ ]$. Near-inertial shear will turn out of alignment with initially-aligned sheets, possibly explaining the nearly-horizontal 0.5-cm laminae consistently observed with a shadowgraph (Laplacian of index of refraction $\nabla^2\eta$) in fingering-favorable parts of the ocean (Kunze *et al*. 1987; St. Laurent and Schmitt 1999). These laminae appear to have horizontal scales consistent with fastest-growing scales. Their small vertical scale would diffusive away molecularly in ~ 4 minutes if they were temperature, and in ~ 8 h if they were salinity, so they must be continuously replenished to be present in the ocean. Using the WKB wavenumber evolution equation

$$\frac{Dk_z}{Dt} = -\,k_x U_z, \qquad (11)$$

Kunze (1990) argued that the observed structure could represent remnant shear-tilted salt microstructure just before it is molecularly diffused away. Fastest-growing fingers that tilt as they grow will have diminishing cross-finger scales, so also diminishing growth rates σ and flux ratios $R_F = \alpha F_T/\beta F_S$.

Kunze (1994) suggested that near-inertial shear might also alter the finger Froude number criterion as a means of explaining towed microstructure measurements. In the staircase east of Barbados, Cox numbers $<(\nabla T)^2>/(<\overline{T_z}>^2)$ were observed to depend linearly on background temperature gradient in the staircase east of Barbados (Fig. 10; Marmorino *et al.* 1987; Fleury and Lueck 1991). This observation implies fluxes independent of interface thickness and background salinity gradient $\overline{S_z}$ while the Stern, or finger Froude, number constraint (8) predicts Cox numbers of ~ 8 independent of interface thickness, and fluxes inversely dependent on interface thickness (9) [linearly dependent on $\overline{S_z}$]. A modified Froude number criterion

$$\frac{U_z w_y}{N^2} \sim O(1) \qquad (13)$$

reproduces the observed Cox numbers, where $U_z = \Delta U/\ell_i$ is the background shear, w_y the finger shear and the velocity step ΔU was observed to be independent of interface thickness. However, arguments for such a criterion are entirely heuristic. A better understanding of how near-inertial shear modifies finger dynamics will be needed to quantify salt-fingering fluxes of heat, salt and momentum in the ocean. A synergy of theory, laboratory and numerical experiments will likely be needed to solve this problem.

8.3. interaction with intermittent shear-driven turbulence

Turbulence produced by internal wave shear is an intermittent process found in 5-10% of the stratified ocean interior. Linden (1971) demonstrated that even very weak turbulence completely disrupts finger fluxes. This result was used by Kunze (1995) to argue that the intermittent turbulence patches lasting about a buoyancy period and arising every 10-20 buoyancy periods in the ocean would allow the more rapidly growing fingers at density ratios $R_\rho < 2.0$ to attain their maximum height (as determined by a finger-Froude-number-like constraint; see section 6), while preventing slower-growing fingers at higher density ratios from reaching their full amplitude. This dramatically reduces fingering fluxes for density ratios $R_\rho > 2$ (Fig. 11) and may help explain why thermohaline staircases are only found at density ratios less than two. The downgradient buoyancy-fluxes associated with high-Reynolds-number turbulence will act to smooth vertical finestructure in contrast to the tendency for countergradient double-diffusive fluxes to sharpen finestructure. Competition between downgradient turbulent and countergradient double-diffusive buoyancy-fluxes may determine whether background stratification is smooth or steppy on finescales.

9. Conclusions and Discussion

Progress has been made in applying salt-fingering theory to ocean observations, and for reconciling differences in results from the ocean observations, laboratory experiments and numerical simulations. However, more rigorous and complete explanations for what controls the fluxes are needed. Many questions remain before we can quantify the role of salt-fingering in mixing the global ocean.

Foremost is determining what limits finger fluxes of heat and salt in the ocean since this has important implications for larger-scale thermohaline circulation. Laboratory $\Delta S^{4/3}$ flux laws apparently do not apply (Gregg and Sanford 1987; Lueck 1987; Hebert 1988). Stern or finger Froude number contraints, while ad hoc, have had success in reproducing some inferred ocean fluxes (Gregg and Sanford 1987; Lueck 1987; Marmorino *et al.* 1987; Hebert 1988; Bianchi *et al.* 2002), and in reconciling lab heat-salt and ocean flux magnitudes. However, they underestimate lab heat-salt fluxes at low density ratios (Fig. 7) and overestimate lab sugar-salt fluxes, suggesting dependence of the fluxes on density ratio R_ρ, Prandtl number ν/κ_T and Lewis number κ_S/κ_T not included in these constraints. They also underestimate recent numerical simulations (Fig. 9) and microstructure-inferred fluxes from the eastern N. Atlantic (St. Laurent and Schmitt 1999), dominated by signals at low density ratio and high Richardson number, suggesting possible additional dependence on finescale internal wave shear and strain, and intermittent shear-driven turbulence. Two-dimensional numerical simulations by Shen (1995) and

Merryfield and Grinder (2000) produce fluxes more compatible with St. Laurent and Schmitt's inferred values
(Fig. 9). Numerical simulations of Radko and Stern (1999; 2000) find fluxes 2-3 times higher in 3-D than in 2-D simulations; this effect is more marked for fingers in uniform background gradients (Radko and Stern (1999) than fingers sandwiched between two convecting layers (Radko and Stern 2000). These discrepancies reveal that we do not yet have a complete dynamical understanding of the processes controlling salt-finger fluxes. A rigorous and complete stability analysis of growing fingers is needed spanning the oceanic, laboratory and numerical parameter space to determine if there is a single stability criterion for the fluxes that can be physically justified and experimentally validated.

Unlike most theoretical, laboratory and numerical considerations of salt fingers, fingers in the ocean co-exist with finescale internal-wave shear of O(N) and strain of O(1), and intermittent internal-wave shear-driven turbulence present in 5-10% of the ocean interior. From the few studies that have investigated interactions between fingers and other oceanic phenomena it is clear that these will affect finger growth, stability, flux ratios and fluxes. Shear tilts fingers, reducing their cross-finger scales, growth rates and possibly their flux ratios. Ad hoc stability criteria involving internal wave and finger shear suggest that higher fluxes may be possible in weak internal wave shear than in fingers alone, possibly explaining the high fluxes inferred by St. Laurent and Schmitt (1999) at low density ratio and high Richardson number in the eastern N. Atlantic. Intermittent turbulence will disrupt the growth of fingers, inhibiting finger fluxes at higher density ratios where fingers grow more slowly. Understanding salt-finger signals in oceanic measurements and correctly inferring heat- and salt-fluxes will undoubtedly require a better understanding of these interactions.

Since salt-finger fluxes depend on the structure of the background stratification, it is also important to determine the mechanisms for forming and maintaining layered finestructure, thermohaline staircases and double-diffusive intrusions. Intrusion theory is well-advanced (Ruddick and Kerr 2000 this issue) and appears to be able to explain ocean observations (Ruddick and Richards 2000 this issue). Both the countergradient buoyancy-flux of salt fingers and double-diffusive intrusions appear to be capable of creating staircase structures but a quantitative prediction for layer and interface thicknesses is still lacking.

Acknowledgments: The author thanks Colin Shen, Timour Radko, Melvin Stern, George Veronis and Bill Merryfield for sharing their insights on salt-fingering theory and making available unpublished manuscripts. This paper is a contribution from SCOR Working Group No. 108 on “Double Diffusion”. E. Kunze was supported by NSF Grant OCE 95-21468.

REFERENCES

Bianchi, A.A., A.R. Piola and G.J. Collino, 2002: Evidence of double diffusion in the Brazil-Malvinas Confluence. *Deep-Sea Res.*, **49**, 41-52.

Boyd, J.D., and H. Perkins, 1987: Characteristics of thermohaline steps off he northwest coast of South America. *Deep-Sea Res.*, **34**, 337-364.

Carmack, E.C., K. Aagaard, J.H. Swift, R.W. Macdonald, F.A. McLaughlin, E.P. Jones, R.G. Perkin, J.N. Smith, K.M. Ellis and L.R. Killius, 1997: Changes in temperature and tracer distributions within the Arctic Ocean: Results from the 1994 Arctic Ocean section. *Deep-Sea Res.*, **44**, 1487-1502.

Padman, L., and T.M. Dillon, 1987: Vertical heat fluxes through the Beaufort Sea thermohaline staircase. *J. Geophys. Res.*, **92**, 10,799-10,806.

Elliott, A.J., M.R. Howe and R.I. Tait, 1974: The lateral coherence of a system of thermohaline layers in the deep ocean. *Deep-Sea Res.*, **21**, 95-107.

Fleury, M., and R. Lueck, 1991: Fluxes across a thermohaline interface. *Deep-Sea Res.*, **38**, 745-769.

Gargett, A.E., and R.W. Schmitt, 1982: Observations of salt fingers in the Central Waters of the eastern North Pacific. *J. Geophys. Res.*, **87**, 8017-8029.

Gregg, M.C., and T.B. Sanford, 1987: Shear and turbulence in thermohaline staircases. *Deep-Sea Res.*, **34**, 1689-1696.

Griffiths, R.W., and B.R. Ruddick, 1980: Accurate fluxes across a salt-sugar interface deduced from direct density measurements. *J. Fluid. Mech.*, **99**, 85-95.

Hebert, D., 1988: Estimates of salt-finger fluxes. *Deep-Sea Res.*, **35**, 1887-1901.

Holyer, J.Y., 1981: On the collective instability of salt fingers. *J. Fluid Mech.*, **110**, 195-207.

Holyer, J.Y., 1984: The stability of long, steady, two-dimensional slat fingers. *J. Fluid Mech.*, **147**, 169-185.

Howard, L.N., and G. Veronis, 1987: The salt-finger zone. *J. Fluid Mech.*, **183**, 1-23.

Howard, L.N., and G. Veronis, 1992: Stability of salt fingers with negligible diffusivity. *J. Fluid Mech.*, **239**, 511-522.

Howe, M.R., and R.I. Tait, 1970: Further observations of thermohaline stratification in the deep ocean. *Deep-Sea Res.*, **17**, 963-972.

Huppert, H.E., and P.C. Manins, 1973: Limiting conditions for salt-fingering at an interface. *Deep-Sea Res.*, **20**, 315-323.

Johannessen, O.M., and O.S. Lee, 1974: A deep stepped thermohaline structure in the Mediterranean. *Deep-Sea Res.*, **21**, 629-639.

Joyce, T.M., 1982: Marginally-unstable salt fingers: Limits to growth. *J. Mar. Res.*, **40** (Suppl.), 291-306.

Kelley, D.E., 1984: Effective diffusivities within oceanic thermohaline staircases. *J. Geophys. Res.*, **89**, 10,484-10,488.

Kunze, E., 1987: Limits on growing, finite-length salt fingers: A Richardson number constraint. *J. Mar. Res.*, **45**, 533-556.

Kunze, E., 1990: The evolution of salt fingers in inertial wave shear. *J. Mar. Res.*, **48**, 471-504.

Kunze, E., 1994: A proposed flux constraint for salt fingers in shear. *J. Mar. Res.*, **52**, 999-1016.

Kunze, E., 1995: Quantifying salt-fingering fluxes in the ocean. in *Double-Diffusive Convection*, A. Brandt and J. Fernando, Eds., AGU Geophysical Monograph 94, 313-320.

Kunze, E., A.J. Williams III and R.W. Schmitt, 1987: Optical microstructure in the thermohaline staircase. *Deep-Sea Res.*, **34**, 1697-1704.

Lambert, R.B., and J.W. Demenkow, 1971: On the vertical transport due to fingers in double-diffusive convection. *J. Fluid Mech.*, **54**, 627-640.

Linden, P.F., 1971: Salt fingers in the presence of grid-generated turbulence. *J. Fluid Mech.*, **49**, 611-624.

Linden, P.F., 1973: On the structure of salt fingers. *Deep-Sea Res.*, **20**, 325-340.

Linden, P.F., 1974: Salt fingers in a steady shear flow. *Geophys. Fluid Dyn.*, **6**, 1-27.

Linden, P.F., 1978: The formation of banded salt-finger structure. *J. Geophys. Res.*, **83**, 2902-2912.

Lueck, R.G., 1987: Microstructure measurements in a thermohaline staircase. *Deep-Sea Res.*, **34**, 1677-1688.

Mack, S.A., 1989: Towed-chain measurements of ocean microstructure. *J. Phys. Oceanogr.*, **19**, 1108-1129.

Mack, S.A., and H.C. Schoeberlein, 1993: Discriminating salt fingernig from turbulence-induced microstructure: Analysis of towed temperature-conductivity chain data. *J. Phys. Oceanogr.*, **23**, 2073-2106.

Magnell, B., 1976: Salt fingers observed in the Mediterranean outflow region (34°N, 11°W) using a towed sensor. *J. Phys. Oceanogr.*, **6**, 511-523.

Marmorino, G.O., 1987: Observations of small-scale mixing processes in the seasonal thermocline: Part I. Salt fingering. *J. Phys. Oceanogr.*, **17**, 1339-1347.

Marmorino, G.O., 1989: Substructure of oceanic salt finger interfaces. *J. Geophys. Res.*, **94**, 4891-4904.

Marmorino, G.O., 1990: "Turbulent mixing" in a salt-finger interface. *J. Geophys. Res.*, **95**, 12,983-12,994.

Marmorino, G.O., W.K. Brown and W.D. Morris, 1987: Two-dimensional temperature structure in the C-SALT thermohaline staircase. *Deep-Sea Res.*, 1667-1676.

Mazeika, P.A., 1974: Subsurface mixed layers in the northwestern tropical Atlantic. *J. Phys. Oceanogr.*, **4**, 446-453.

McDougall, T.J., 1991: Interfacial advection in the thermohaline staircase east of Barbados. *Deep-Sea Res.*, **38**, 357-370.

McDougall, T.J., and J.R. Taylor, 1984: Flux measurements across a finger interface at low values of the stability ratio. *J. Mar. Res.*, **42**, 1-14.

Merryfield, W.J., 2000: Origin of thermohaline staircases. *J. Phys. Oceanogr.*, **30**, 1046-1068.

Merryfield, W.J., and M. Grinder, 2000: Salt-fingering fluxes from numerical simulations. *J. Phys. Oceanogr.*, submitted.

Miles, J.W., and L.N. Howard, 1961: On the stability of heterogeneous shear flows. *J. Fluid Mech.*, **10**, 496-512.

Özgökmen, T.M., O.E. Esenkov and D.B. Olson, 1998: A numerical study of layer formation due to fingers in double-diffusive convection in a vertically-unbounded domain. *J. Mar. Res.*, **56**, 463-487.

Proctor, M.R.E., and J.Y. Holyer, 1986: Planform selection in salt fingers. *J. Fluid Mech.*, **168**, 241-253.

Radko, T., and M.E. Stern, 1999: Salt fingers in three dimensions. *J. Mar. Res.*, **57**, 471-502.

Radko, T., and M.E. Stern, 2000: Finite-amplitude salt fingers in a vertically bounded layer. *J. Fluid Mech.*, **425**, 133-165.

Ruddick, B., and O. Kerr, 2000: Oceanic thermohaline intrusions: Theory. *Prog. Oceanogr.*, this issue (submitted).

St. Laurent, L., and R.W. Schmitt, 1999: The contribution of salt fingers to vertical mixing in the North Atlantic Tracer Release Experiment. *J. Phys. Oceanogr.*, **29**, 1404-1424.

Schmitt, R.W., 1979a: Flux measurements in an interface. *J. Mar. Res.*, **37**, 419-436.

Schmitt, R.W., 1979b: The growth rate of supercritical salt fingers. *Deep-Sea Res.*, **26A**, 23-44.

Schmitt, R.W., 1994: Triangular and asymmetric salt fingers. *J. Phys. Oceanogr.*, **24**, 855-860.

Schmitt, R.W., 1995: The ocean's salt fingers. *Sci. Amer.*, **272**(5), 50-55.

Schmitt, R.W., 2000: Observational evidence for salt fingers. *Prog. Oceanogr.*, this issue (submitted).

Schmitt, R.W., H. Perkins, J.D. Boyd and M.C. Stalcup, 1987: C-SALT: An investigation of the thermohaline staircase in the western tropical North Atlantic, *Deep-Sea Res.*, **34**, 1655-1666.

Shen, C.Y., 1989: The evolution of the double-diffusive instability: Salt fingers. *Phys. Fluids A*, **1**, 829-844.

Shen, C.Y., 1993: Heat-salt finger fluxes across a density interface. *Phys. Fluids A*, **5**, 2633-2643.

Shen, C.Y., 1995: Equilibrium salt-fingering convection. *Phys. Fluids*, **7**, 706-717.

Shen, C.Y., and R.W. Schmitt, 1995: The salt-finger wavenumber spectrum. in *Double-Diffusive Convection*, A. Brandt and J. Fernando, Eds., AGU Monograph 94, 305-312.

Shen, C.Y., and G. Veronis, 1997: Numerical simulation of two-dimensional salt fingers. *J. Geophys. Res.*, **102**, 23,131-23,143.

Stamp, A.P., G.O. Hughes, R.I. Nokes and R.W. Griffiths, 1998: The coupling of waves and convection. *J. Fluid Mech.*, **372**, 231-271.

Stern, M.E., 1960: The "salt-fountain" and thermohaline convection. *Tellus*, **12**, 172-175.

Stern, M.E., 1969: Collective instability of salt fingers. *J. Fluid Mech.*, **35**, 209-218.

Stern, M.E., 1975: Ocean Circulation Physics. Academic Press, NY, 191-203.

Stern, M.E., 1976: Maximum buoyancy-flux across a salt-finger interface. *J. Mar. Res.*, **34**, 95-110.

Stern, M.E., T. Radko and J. Simeonov, 2001: 3-D salt fingers in an unbounded thermocline with application to the Central Ocean. *J. Mar. Res.*, **59**, 355-390.

Stern, M.E., and J.S. Turner, 1969: Salt fingers and convecting layers. *Deep-Sea Res.*, **16**, 497-511.

Taylor, J.R., and P. Bucens, 1989: Laboratory experiments on the structure of salt fingers. *Deep-Sea Res.*, **36**, 1675-1704.

Thangam, S., A. Zebib and C.F. Chen, 1984: Salt-finger convection in shear flow. *Phys. Fluids*, **27**, 804-811.

Turner, J.S., 1967: Salt fingers across a density interface. *Deep-Sea Res.*, **14**, 599-611.

Yoshida, J., and H. Nagashima, 2000: Numerical simultions of salt-fingers. *Prog. Oceanogr.*, this issue, submitted.

Walsh, D., and B.R. Ruddick, 1995: An investigation of Kunze's salt-finger flux laws – Are they stable? *Double-Diffusive Convection*, *Geophys. Monogr.*, No. 94, Amer. Geophys. Union, 321-328.

Walsh, D., and B. Ruddick, 2000: Double-diffusive interleaving in the presence of turbulence: The effect of a nonconstant flux ratio. *J. Phys. Oceanogr.*, **30**, 2231-2245.

Winters, K.B., and E.A. D'Asaro, 1996: Diascalar flux and the rate of fluid mixing. *J. Fluid Mech.*, **317**, 179-193.

Zodiatis, G., and G.P. Gasparini, 1996: Thermohaline staircase formations in the Tyrrhenian Sea. *Deep-Sea Res.*, **43**, 655-678.

Table 1: Parameter values typical of the thermohaline staircase east of Barbados.

Variable	Value
ν	10^{-6} m^2 s^{-1}
κ_T	1.4×10^{-7} m^2 s^{-1}
κ_S	1.1×10^{-9} m^2 s^{-1}
g	9.8 m s^{-2}
α	2×10^{-4} °C^{-1}
β	7.5×10^{-4} psu^{-1}
L_o	20 m
ℓ_i	2 m
$\overline{T}_z$	0.3 °C m^{-1}
$\overline{S}_z$	0.05 psu m^{-1}
N	1.5×10^{-2} rad s^{-1}
$P_N = 2\pi/N$	7 min
R_ρ	1.6
λ_{fg}	3.1 cm
U_z	6.3×10^{-3} rad s^{-1}
f	3.5×10^{-5} rad s^{-1}
$P_f = 2\pi/f$	2 days
Ri	6

FIGURE CAPTIONS

Figure 1: Contours of salt-finger growth rate σ normalized by buoyancy frequency N for parameter values typical of the high-gradient interfaces in the thermohaline staircase east of Barbados (Table 1) as a function of finger wavelength λ and background density ratio $1 < R_\rho = \alpha \overline{T}_z/(\beta \overline{S}_z) < 2$. Growth rates are negative (decay) for wavelengths λ less than 0.8 cm and positive for larger wavelengths, but only exceed the buoyancy frequency $N = \sqrt{g\beta\overline{S}_z(R_\rho - 1)}$ at very low density ratios. The dotted curve displays the wavelength of maximum growth rate as a function of density ratio.

Figure 2: Contours of flux ratio $R_F = \langle w\alpha T'\rangle/\langle w\beta S'\rangle$ as a function of finger wavelength λ and density ratio R_ρ. The dotted curve is the wavelength of maximum growth rate as a function of density ratio. The flux ratio R_F increases from 0 for vanishing growth rate to 0.85 for low density ratios and larger wavelengths. Steady fingers lie near $\lambda = 0.8$ cm, implying flux ratios less than 0.05 (see Fig. 3).

Figure 3: Salt-finger flux ratio $R_F = \langle w\alpha T'\rangle/\langle w\beta S'\rangle$ vs. density ratio R_ρ. Symbols are from laboratory (solid symbols) and numerical simulation (open symbols) estimates, the solid curve for theoretical fastest-growing fingers and the dashed curve for steady ($\sigma = 0$) fingers.

Figure 4: An example of numerical simulation of growing salt fingers in a thin interface (Shen 1993). The resulting structure does not resemble the tall thin fingers of theoretical treatments but quickly becomes nearly isotropic and blob-like.

Figure 5: Theoretical wavelengths λ as a function of density ratio R_ρ for fastest-growing (solid) and steady (dashed) fingers using typical properties of interfaces in the thermohaline staircase east of Barbados (Table 1).

Figure 6: Maximum theoretical finger growth rates σ (solid) as a function of density ratio R_ρ for interfaces in the thermohaline staircase east of Barbados (Table 1). Also shown are buoyancy frequencies N (dashed) and molecular viscous and diffusive timescales (dotted).

Figure 7: Theoretical heat (dashed), salt (dotted) and total negative (solid) buoyancy-fluxes as a function of density ratio R_ρ, assuming that the maximum finger amplitude is constrained by a critical finger Froude number $Fr_C = |\nabla w|/N = 2.0$. The upper panel assumes an interface thickness ℓ_i of 2 m, consistent with observed values. The central panel assumes an interface thickness ℓ_i identical to the maximum finger height h_{max}, producing interface thicknesses of ~O(10 cm) and higher fluxes as a result. The bottom panel normalizes these fluxes by a $\Delta S^{4/3}$ flux law and compares the salt-flux (dotted) with c values from laboratory and numerical experiments (symbols). The model reproduces the laboratory values at density ratios $R_\rho > 2$ but underestimates fluxes at low density ratios R_ρ.

Figure 8: Flux ratio R_F (a), $\Delta S^{4/3}$ flux law coefficient c (b) and Stern number A (c) as a function of density ratio from numerical simulations (solid diamonds) and lab experiments (other symbols) (from Shen 1993). Laboratory and numerical model numbers are consistent with each other and indicate that the critical Stern number is not an invariant.

Figure 9: Finger-induced salt diffusivities K_S as a function of density ratio R_ρ in a uniform background vertical gradient from a Stern-number constraint (9-10) (dotted curve) and from 2- and 3-D numerical simulations (symbols). The dependence on density ratio differs markedly in the two approaches, with the numerical simulations implying much higher eddy diffusivities for density ratios $R_\rho < 3$.

Figure 10: Temperature Cox numbers C_T versus vertical temperature-gradients $\overline{T_z}$ in interfaces of the thermohaline staircase east of Barbados. Data are from (a) a towed microscale conductivity cell (Marmorino 1989) and (b) a towed microthermistor (Fleury and Lueck 1991). Solid dots in (a) denote the mean of the distribution, open circles the mode. Only means are displayed in (b). In both data sets, mean Cox numbers C_T are roughly proportional to $\overline{T_z}^{-1}$.

Figure 11: Alternative theoretical finger salt diffusivities K_S as a function of density ratio R_ρ. The solid curve assumes a finger Froude number constraint $Fr_c = |\nabla w|/N = 2.0$, the thin dashed curve a mixed finger/wave Froude number $U_z w_y/N^2 = 2.0$ with wave shear $U_z = 0.6N$, and the thick dashed curve represents the diffusivity relative to gradients smoothed over a staircase $-<w'S'>/<\bar{S_z}>$. Dotted curves correspond to diffusivities where finger growth is squelched by intermittent internal-wave-driven turbulence every 10 buoyancy periods. A plausible scenario for the ocean is that (i) at high density ratios ($R_\rho > 2.4$), finger growth is inhibited by turbulence rather than self secondary instability (dotted curves), while, (ii) at low density ratios ($R_\rho <$ 1.6), finger countergradient buoyancy-fluxes overcome turbulent downgradient buoyancy-fluxes (stippling) so that staircases form, producing high-gradient interfaces and amplifying fluxes (thick dashed). At intermediate density ratios, finger diffusivities will lie between the thin dashed and thick solid curves, depending on the strength of the internal wave shear U_z. The resulting hydrid curve resembles Fig. 5 of Schmitt (1981), albeit a factor of 30 lower.

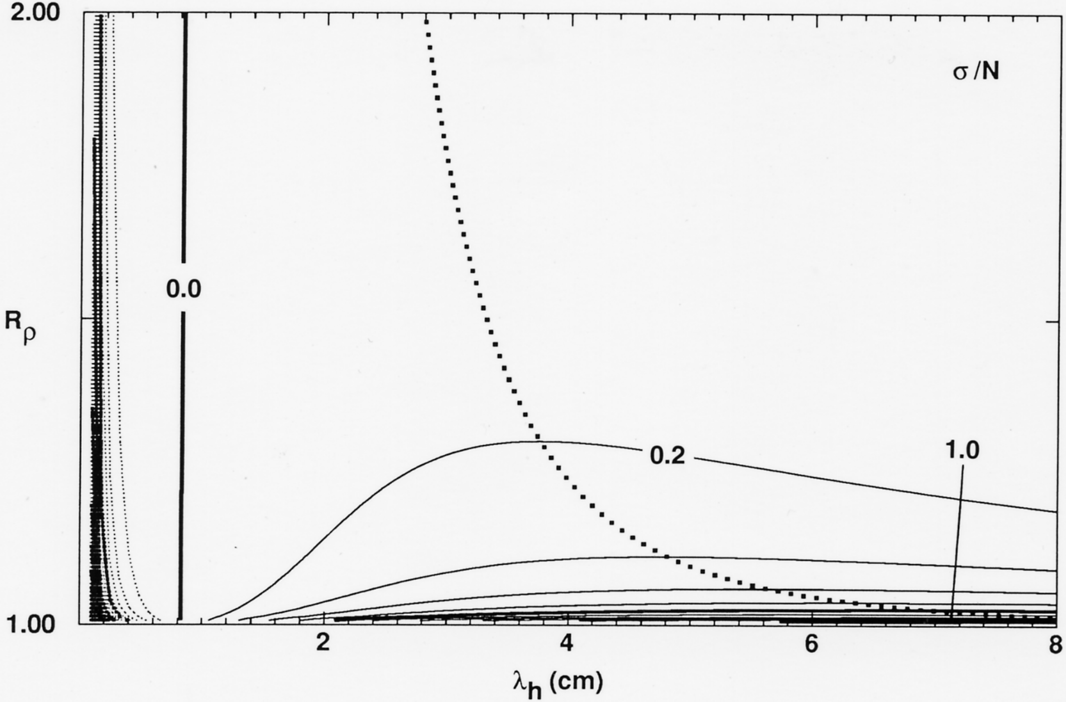

2.00
1.00
R_ρ
σ /N
0.0
0.2
1.0
2
4
6
8
λ_h (cm)

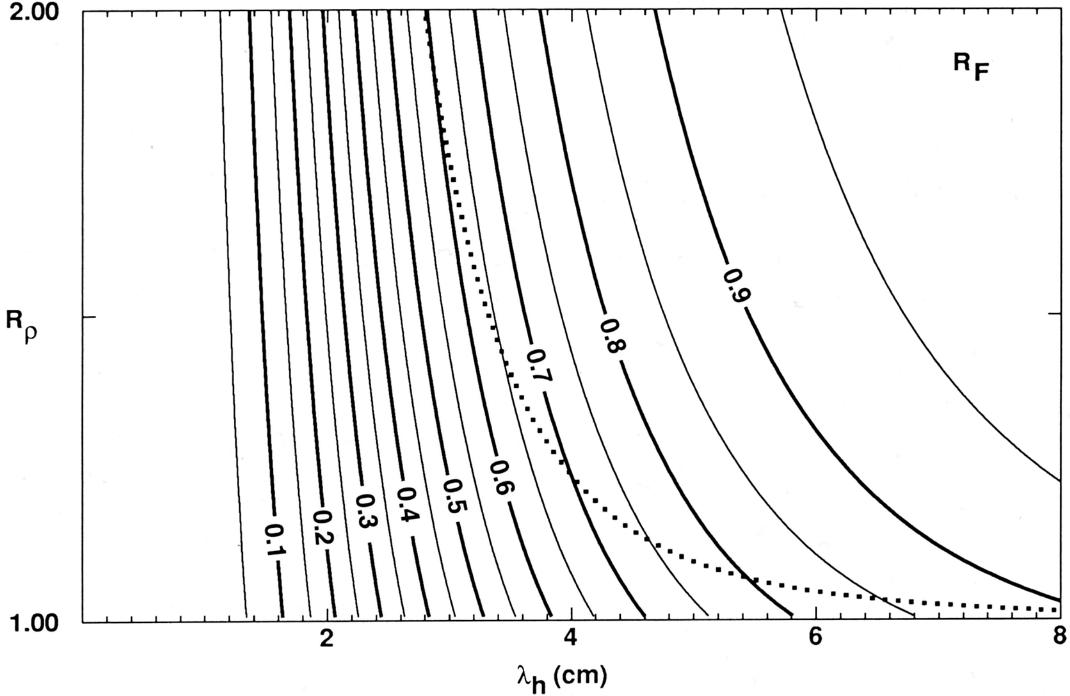

2.00
1.00
R_ρ
R_F
0.1
0.2
0.3
0.4
0.5
0.6
0.7
0.8
0.9
2
4
6
8
λ_h (cm)

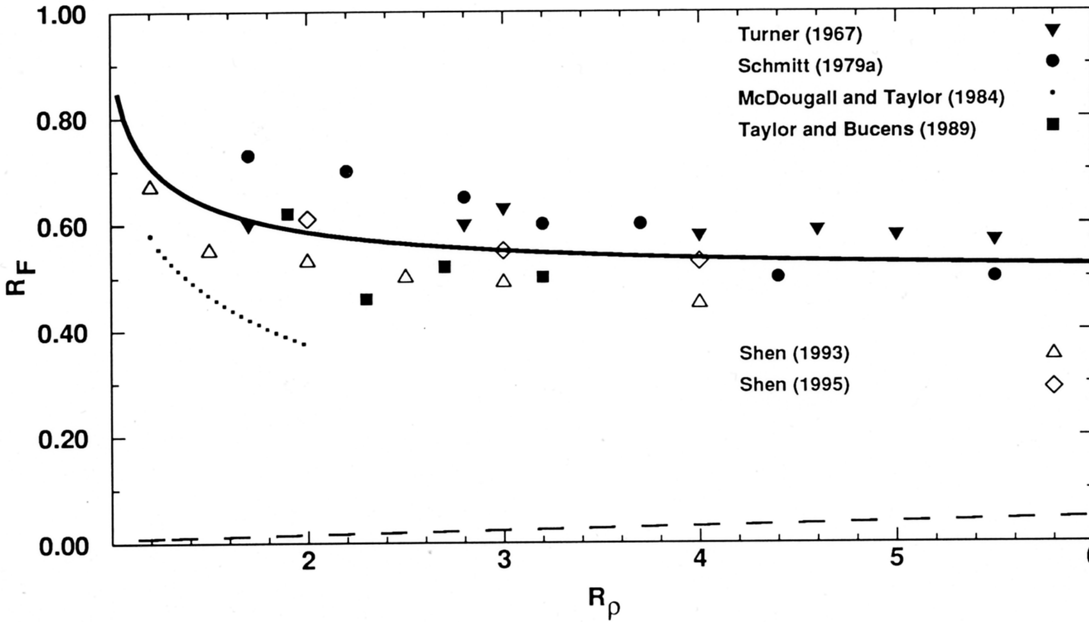

1.00
0.80
0.60
0.40
0.20
0.00
2
3
4
5
6
R_F
R_ρ
Turner (1967)
Schmitt (1979a)
McDougall and Taylor (1984)
Taylor and Bucens (1989)
Shen (1993)
Shen (1995)

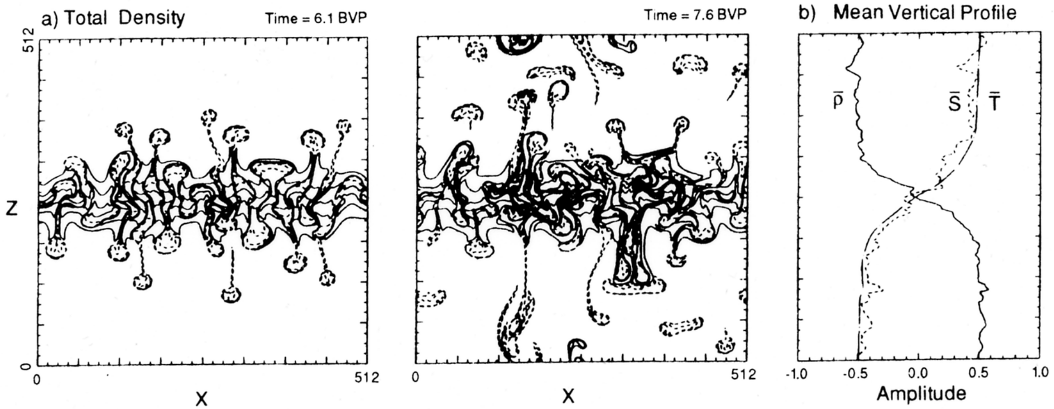
a) Total Density
Time = 6.1 BVP
Time = 7.6 BVP
512
0
Z
X
0
512
0
512
X
b) Mean Vertical Profile
$\bar{\rho}$
$\bar{S}$
$\bar{T}$
-1.0
-0.5
0.0
0.5
1.0
Amplitude

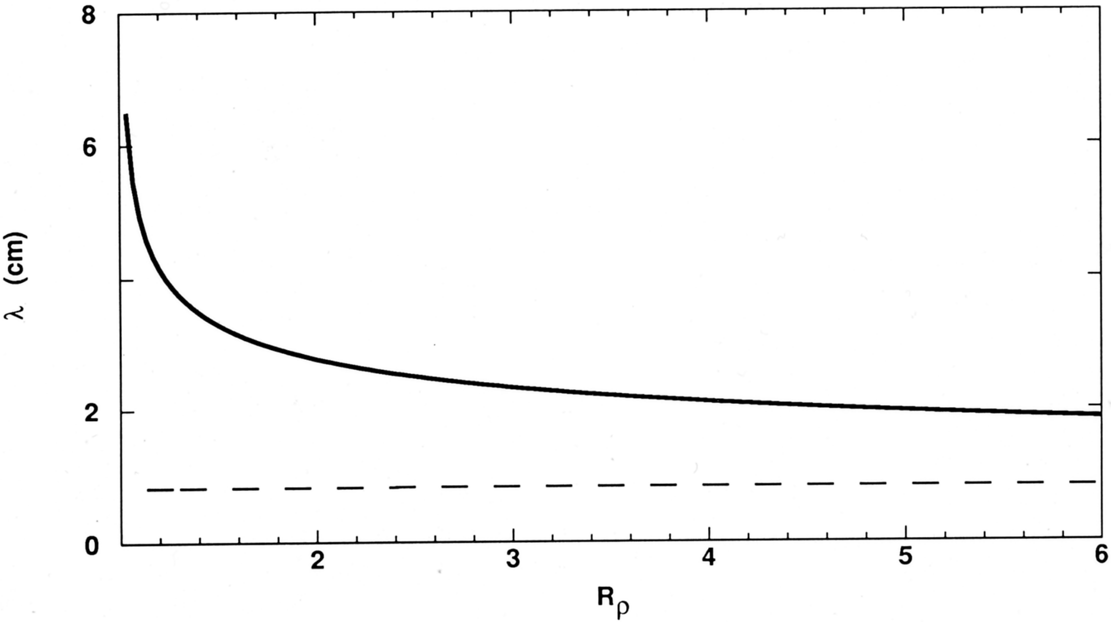

8
6
2
0
2
3
4
5
6
λ (cm)
R_ρ

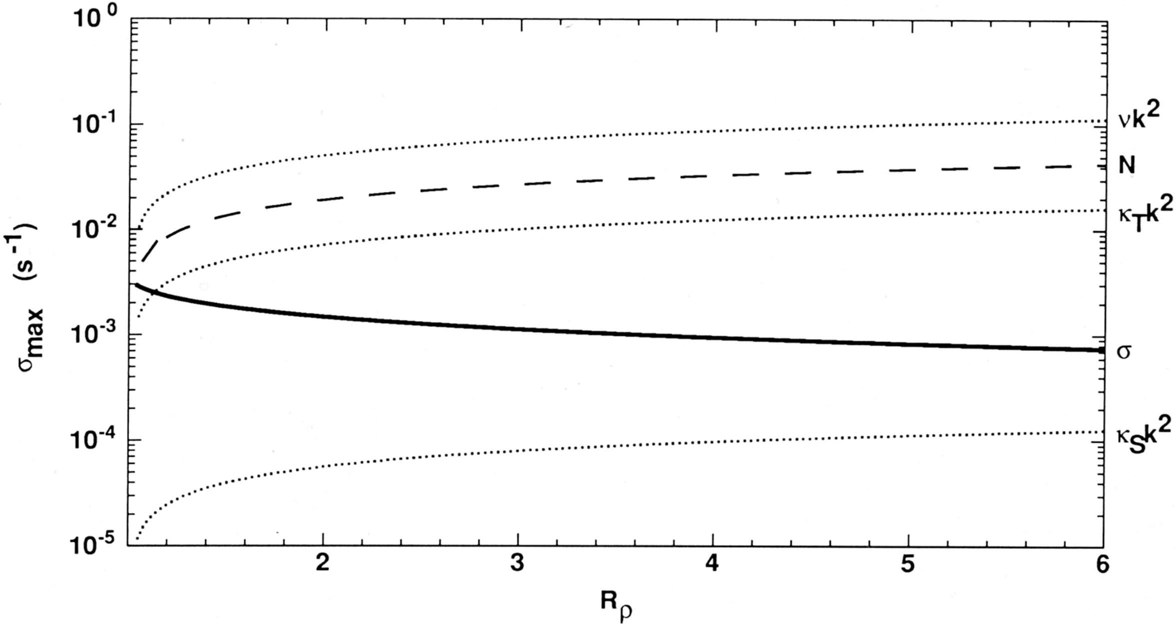

10^0
10^{-1}
10^{-2}
10^{-3}
10^{-4}
10^{-5}
σ_{max} (s^{-1})
2
3
4
5
6
R_ρ
νk^2
N
$\kappa_T k^2$
σ
$\kappa_S k^2$

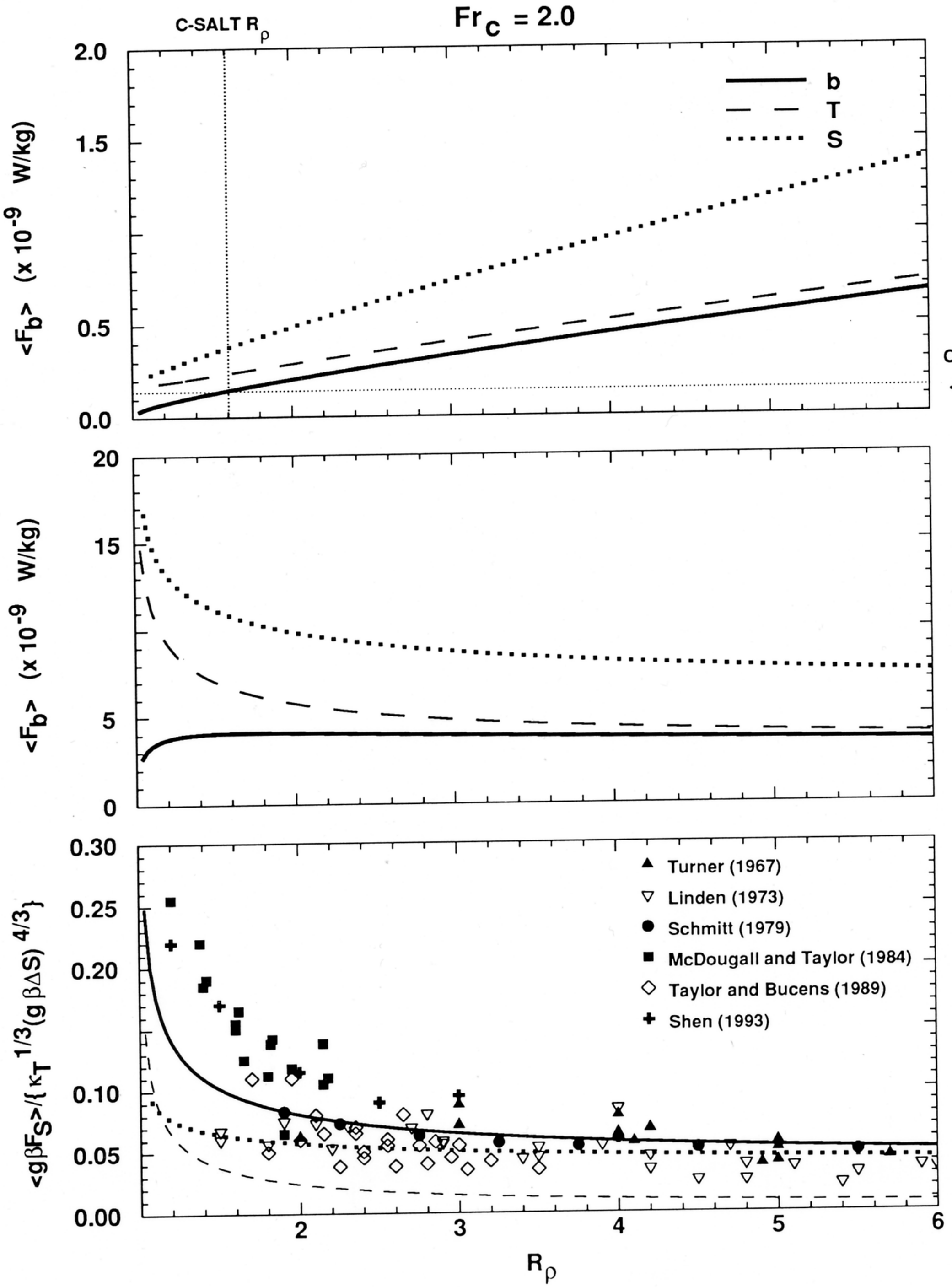

Fr$_C$ = 2.0
C-SALT R$_\rho$
2.0
1.5
0.5
0.0
b
T
S
<F$_b$> (x 10^{-9} W/kg)
C-SALT
<F$_b$>
20
15
5
0
<F$_b$> (x 10^{-9} W/kg)
0.30
0.25
0.20
0.10
0.05
0.00
Turner (1967)
Linden (1973)
Schmitt (1979)
McDougall and Taylor (1984)
Taylor and Bucens (1989)
Shen (1993)
<gβF$_S$>/{κ$_T$$^{1/3}$(gβΔS)$^{4/3}$}
2
3
4
5
6
R$_\rho$

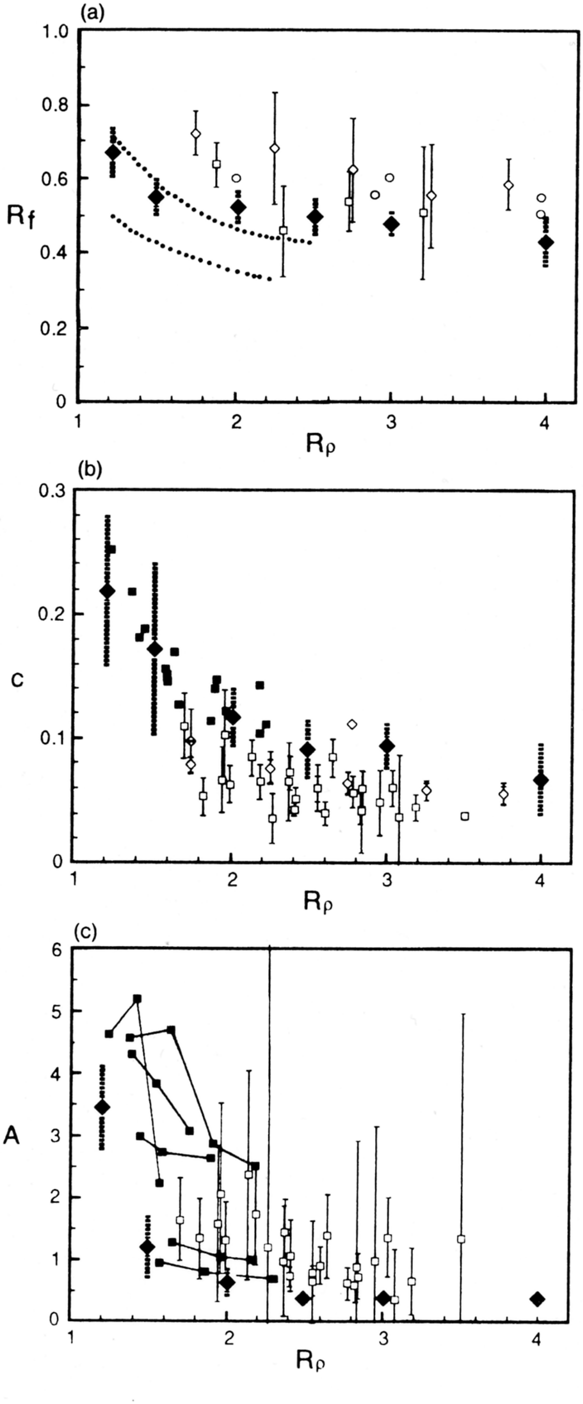

(a)
1.0
0.8
0.6
0.4
0.2
0
R_f
1
2
3
4
R_ρ
(b)
0.3
0.2
0.1
0
c
1
2
3
4
R_ρ
(c)
6
5
4
3
2
1
0
A
1
2
3
4
R_ρ

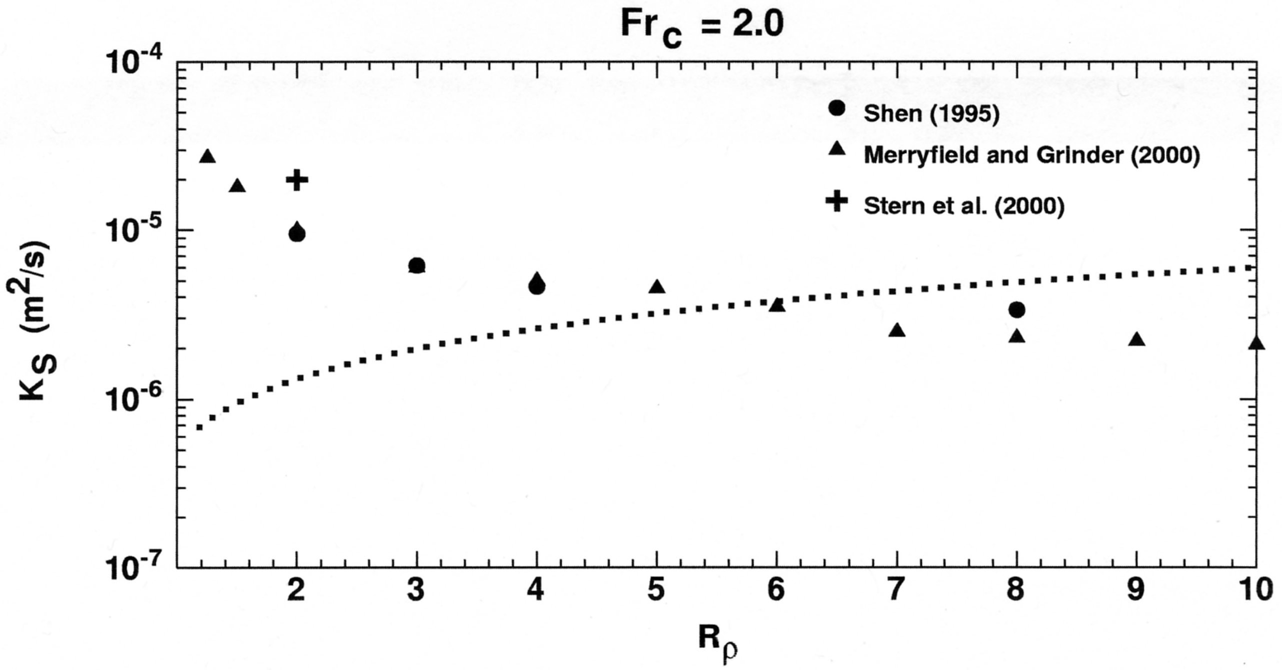

Fr_C = 2.0
10^-4
10^-5
10^-6
10^-7
K_S (m^2/s)
Shen (1995)
Merryfield and Grinder (2000)
Stern et al. (2000)
2
3
4
5
6
7
8
9
10
R_ρ

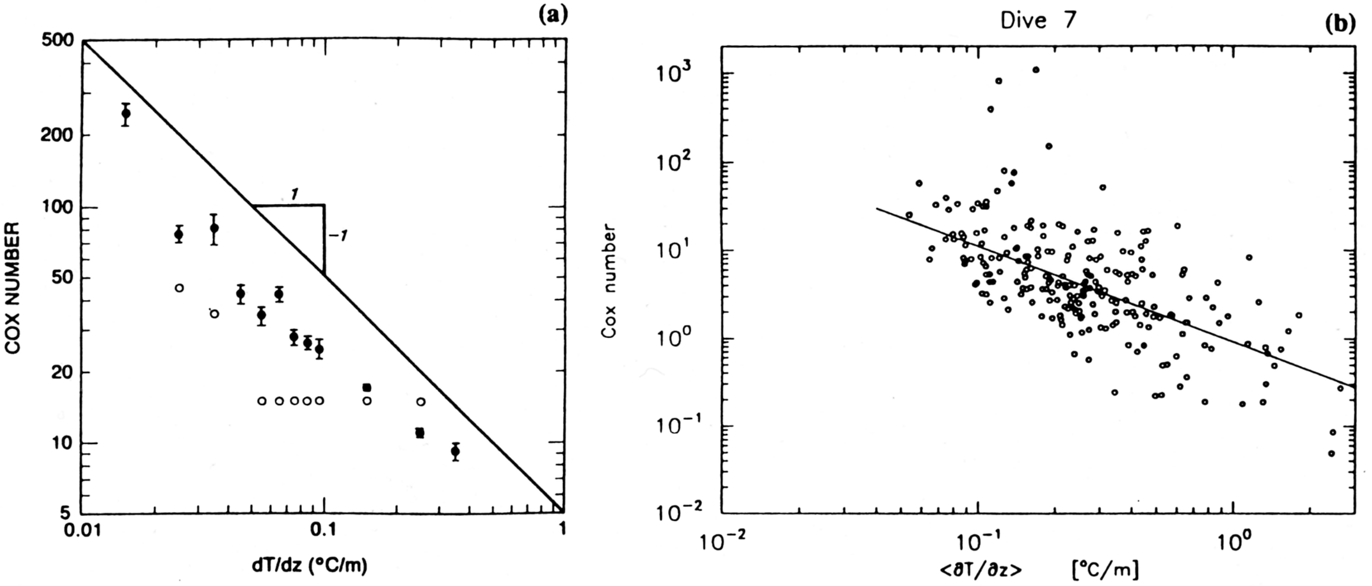
(a)
COX NUMBER
500
200
100
50
20
10
5
0.01
0.1
1
1
−1
dT/dz (°C/m)
Dive 7
(b)
Cox number
10^3
10^2
10^1
10^0
10^{-1}
10^{-2}
10^{-2}
10^{-1}
10^0
<∂T/∂z> [°C/m]

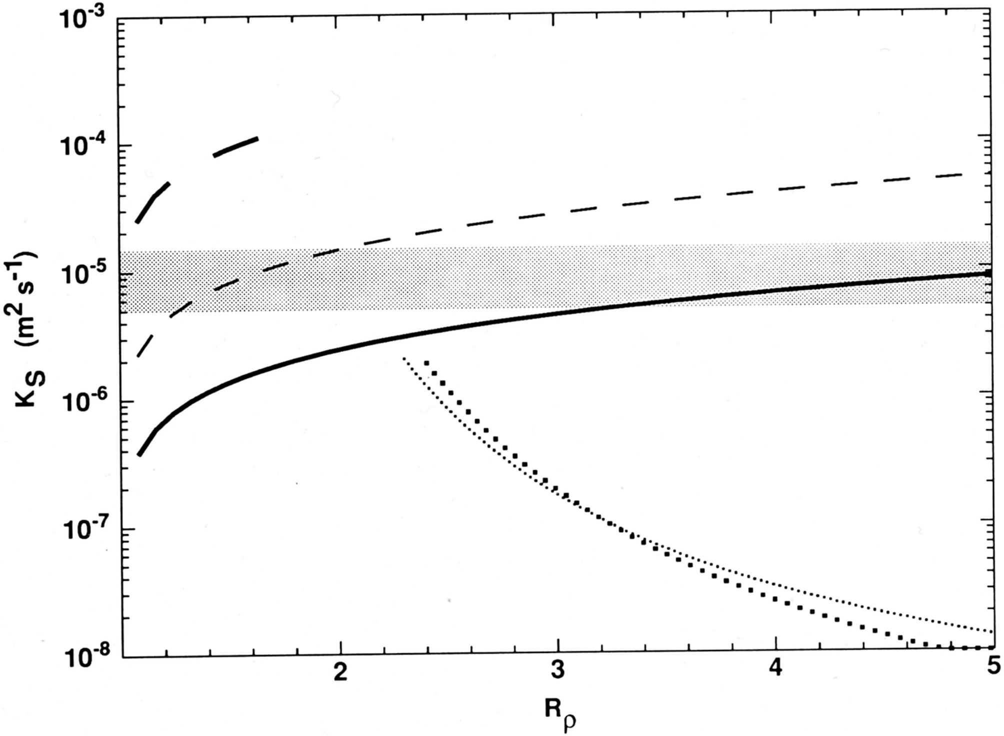

10-3
10-4
10-5
10-6
10-7
10-8
K_S (m^2 s^-1)
2
3
4
5
R_ρ